Heliyon 9 (2023) e17889

Contents lists available at ScienceDirect

Heliyon

journal homepage: www.cell.com/heliyon

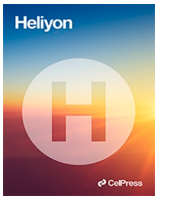

Fabrication and electrochemical properties of electrode composites for oxide-type all-solid-state batteries through electrostatic integrated assembly

Kazuhiro Hikima [a], Yusaku Sato [a], Atsushi Yokoi [b], Wai Kian Tan [b], Hiroyuki Muto [a,b], Atsunori Matsuda [a,*]

[a] Department of Electrical and Electronic Information Engineering, Toyohashi University of Technology, 1-1 Hibarigaoka, Tempaku, Toyohashi, Aichi 441-8580, Japan
[b] Institute of Liberal Arts and Sciences, Toyohashi University of Technology, 1-1 Hibarigaoka, Tempaku, Toyohashi, Aichi 441-8580, Japan

ARTICLE INFO

Keywords:
Electrostatic integrated assembly method
Carbon nanotube
Oxide-type solid electrolyte
Lithium oxide cathode

ABSTRACT

All-solid-state batteries, which use flame-resistant solid electrolytes, are regarded as safer alternatives to conventional lithium-ion batteries for various applications including electric vehicles. Herein, we report the fabrication of cathode composites for oxide-type all-solid-state batteries through an electrostatic assembly method. A polyelectrolyte is used to adjust the surface charge of the matrix particles to positive/negative, and the aggregation resulting from electrostatic interactions is utilized. Composites consisting of cathode active material particles ($LiNi_{1/3}Mn_{1/3}Co_{1/3}O_2$ (NMC) or $LiNi_{0.5}Mn_{1.5}O_4$ (LNMO)), solid electrolyte particles $Li_{1.3}Al_{0.3}Ti_{1.7}(PO_4)_3$ (LATP), and electron conductive one-dimensional carbon nanotubes (CNT) are formed via an electrostatic integrated assembly of colloidal suspensions. Electrostatic integration increases the electronic conductivity by two orders of magnitude in the NMC–LATP–CNT composite (6.5×10^{-3} S cm^{-1}/3.2×10^{-5} S cm^{-1}) and by six orders of magnitude in the LNMO–LATP–CNT composite (6.4×10^{-3} S cm^{-1}/2.3×10^{-9} S cm^{-1}). The dispersion of CNTs in the cathode composite is enhanced, resulting in percolation of e^- path even at 1 wt% (approximately 2.5 vol %) CNT. This study indicates that an integrated cathode composite can be fabricated with particles uniformly mixed by electrostatic interaction for oxide-type all-solid-state batteries.

1. Introduction

Secondary batteries are used in various electronic devices and are indispensable to everyday life. Environmental issues have increased the demand for electric vehicles and batteries with higher energy densities. Accordingly, high-energy-density lithium-ion secondary batteries have been used to satisfy these requirements. However, lithium-ion batteries contain flammable organic solvents as electrolytes, which increases the risk of overcharging or short circuits. All-solid-state batteries, which use flame-resistant solid electrolytes, are considered relatively safe. All-solid-state batteries can be primarily divided into two types of sulfide and oxide.

The ionic conductivities of sulfide materials are reported to be generally higher than those of oxide materials. In addition, owing to their high ionic conductivity and plastic deformation at room temperature, sulfide solid electrolytes can effectively form a good

* Corresponding author.
E-mail address: matsuda@ee.tut.ac.jp (A. Matsuda).

https://doi.org/10.1016/j.heliyon.2023.e17889
Received 18 April 2023; Received in revised form 27 June 2023; Accepted 30 June 2023
Available online 3 July 2023

interface with electrode active materials [1]. The conductivities (10^{-4}–10^{-2} S cm^{-1}) of various sulfide materials, such as $Li_{10}GeP_2S_{12}$ (1.2×10^{-2} S cm^{-1} at room temperature) [2] and $Li_7P_3S_{11}$ (1.0×10^{-2} S cm^{-1} at room temperature) [3], are comparable to those of organic electrolytes. However, sulfide materials usually react with moisture in the atmosphere to produce toxic H_2S.

In contrast, oxide solid electrolytes are chemically stable and can be safely used in air. In addition, a thin-film-type oxide-based all-solid-state battery has been found to considerably improve the battery characteristics, although its oxide-type cathodes (for example, Li-rich-type cathodes such as Li_2MnO_3) cannot be easily used in organic electrolyte-based batteries because of the continuous decomposition of the organic electrolyte in the high-voltage region, and the structural deterioration with the dissolution of transition metal and/or oxygen removal [4,5,6]. To expand the application from thin-film-type to practical powder-type batteries, cathode composites must be fabricated by mixing a cathode active material, solid electrolyte, and conductive additive. In addition, sintering at high temperatures is necessary for densification, porosity reduction, and the formation of ion-conducting paths [7,8,9]. In an all-solid-state battery, the contact between a cathode active material and a solid electrolyte is critical because the ion transfer occurs through the solid electrolyte. However, the cathode active material and solid electrolyte are composed of sub-micron to micro-sized particles, whereas the conductive additive particles are nano-sized; therefore, material agglomeration is a problem encountered during dry mixing [10,11]. One of the solutions involves using the liquid-phase method, in particular electrostatic integrated assembly [12], for fabricating well-dispersed cathode composites due to easier integration of nano-sized materials with exhibiting improved homogeneity. However, the application of an electrostatic integrated assembly to prepare cathode composites with lithium-containing oxides for oxide-type all-solid-state batteries has not been reported thus far.

In this study, cathode composites were prepared through an electrostatic integrated assembly [12], and sintered at various temperatures; moreover, the electronic and ionic conductivities of the composites were evaluated. NASICON-type $Li_{1.3}Al_{0.3}Ti_{1.7}(PO_4)_3$ (LATP), which is an oxide solid electrolyte, was used because of its high chemical stability, electrochemical stability at high voltage region, and ionic conductivity at room temperature [13,14,15,16,17]. In addition, $LiNi_{1/3}Mn_{1/3}Co_{1/3}O_2$ and $LiNi_{0.5}Mn_{1.5}O_4$ were used as representative cathode active materials, and carbon nanotubes (CNTs) were used as an electron conductive carbon source. Methanol (MeOH) was used as the solvent instead of water, because the exposure of LATP to water considerably decreases the ionic conductivity and results in lithium dissolution and unit cell shrinkage [18]. We demonstrate the formation of integrated composites consisting of cathode active material particles ($LiNi_{1/3}Mn_{1/3}Co_{1/3}O_2$ or $LiNi_{0.5}Mn_{1.5}O_4$), LATP solid electrolyte particles, and electron conductive one-dimensional CNTs via an electrostatic integrated assembly of colloidal suspensions.

2. Experimental

2.1. Composite preparation via mortar mixing

The cathode active materials, $LiNi_{1/3}Mn_{1/3}Co_{1/3}O_2$ (NMC; average particle size = 1 μm, TODA KOGYO CORP.) or $LiNi_{0.5}Mn_{1.5}O_4$ (LNMO; average particle size = 1 μm, Toshima Manufacturing Co., Ltd.), $Li_{1.3}Al_{0.3}Ti_{1.7}(PO_4)_3$ (LATP; average particle size = 1 μm, Toshima Manufacturing Co., Ltd.), and CNTs (average diameter = 2 nm and average length = 1 μm, OCSiAl) were weighed at a ratio of cathode active material:LATP:CNT = 33:66:1(wt%) and hand-mixed for 15 min using an agate mortar for composite formation. Fig. S1 depicts the scanning electron microscopy (SEM) images of the starting materials: NMC, LNMO, LATP, and CNTs.

2.2. Composite preparation via electrostatic integration

Suspensions of each material were prepared for fabricating the composites via electrostatic integration. Initially, LATP and CNT were dispersed by ultrasonic in 1 wt% poly(diallydimethyl ammonium chloride) (PDDA; Sigma–Aldrich) dissolved in MeOH. To remove excess PDDA, the suspension was washed several times with MeOH after centrifugation [10,12]. Subsequently, NMC and LNMO particles were immersed in the PDDA solution and mixed ultrasonically. The PDDA-coated NMC and LNMO particles were dispersed in 1 wt% poly(acrylic acid) (PAA; FUJIFILM Wako Pure Chemical Corporation) dissolved in MeOH. A multilayer film of PDDA–PAA was formed on the NMC and LNMO surfaces, resulting in a negatively charged suspension. Each suspension was transferred to a screw tube at a weight ratio of cathode active material (NMC or LNMO):LATP:CNT = 33:66:1(wt%) (approximately 22.9:74.6:2.5 (vol%)) and rotated to produce composite powders. The cathode composite was dried in a drying oven at 80 °C for 1 h to remove MeOH. Furthermore, for the NMC–LATP–CNT composite, other composite ratios such as NMC:LATP:CNT = 44.5:44.5:1 (approximately 36.8:60.2:3.0 (vol%)) and 69.3:29.7:1.0(wt%) (approximately 57.0:40.0:3.0 (vol%)) were prepared.

2.3. Characterization

The zeta potential of each material and cathode composite was measured using zeta potential measuring equipment (ELSZ-1, Otsuka Electronics). The crystal structures of the cathode composites were evaluated via powder X-ray diffraction (XRD; Ultima IV, Rigaku) with CuKα radiation (40 kV, 30 mA). A field emission scanning electron microscope (FE-SEM; S-4800, Hitachi) were used for observing the morphology of the cathode composites.

2.4. Electrochemical properties

The NMC–LATP–CNT and LNMO–LATP–CNT composites prepared via mortar mixing were each weighed at 80 mg and compacted in a uniaxial press at 300 MPa for 15 min. The composites were sintered for 5 h in a nitrogen flow tube furnace at 650, 750, or 800 °C.

The sintered composites were placed in a polyether ether ketone cell, and a direct current (DC) polarization test (1260A, Solartron Analytical) with SUS/Composites/SUS (ion blocking electrode) was conducted to measure the electronic conductivity at room temperature. The DC polarization test with the SUS/argyrodite solid electrolyte/Composites/argyrodite solid electrolyte/SUS cell (electron blocking electrode) was also conducted at 90 °C to measure the ionic conductivity. The argyrodite solid electrolyte exhibited an ionic conductivity of 2.8×10^{-3} S cm^{-1} at room temperature. This synthesis procedure was utilized in a previous study [19]. The ionic conductivity was calculated from the resistance value of the entire argyrodite solid electrolyte/composites/argyrodite solid electrolyte. Then, the resistance values from the argyrodite solid electrolytes were excluded to calculate the composites resistance.

3. Results and discussion

3.1. Composite preparation and characterization

Table S1 lists the zeta potentials of each suspension. After surface treatment by PDDA, suspensions of LATP and CNT particles exhibited positive zeta potentials of approximately +49 and + 58 mV, respectively. In addition, a multilayer film of PDDA–PAA on the NMC and LNMO surface presented negatively charged zeta potentials of −54 and −37 mV, respectively. Particularly, the zeta potential after mixing was adjusted to within ±15 mV to prepare composites via electrostatic integration. Fig. 1 depicts the SEM images of each composite. For the NMC–LATP–CNT (Fig. 1(a)) and LNMO–LATP–CNT (Fig. 1(b)) composites, which were prepared via mortar mixing, CNTs were predominantly aggregated. However, for the NMC–LATP–CNT (Fig. 1(c)) and LNMO–LATP–CNT (Fig. 1(d)) composites fabricated via electrostatic integration, CNTs were found to be dispersed on the particle surface. Fibrous CNTs have a higher cohesive force than that of fine particles owing to the surface cohesive force. Therefore, mortar mixing presented insufficient energy for dispersion. In contrast, during the surface charge adjustment of CNTs, the ultrasonic dispersion of CNTs and PDDA adsorption on the surface led to CNTs dispersion owing to electrostatic repulsion. Consequently, the CNTs were dispersed in the solvent, and the dispersibility was enhanced owing to electrostatic repulsion and effects of cross-linking.

Fig. 2 and S2 present the XRD patterns of the NMC–LATP–CNT and the LNMO–LATP–CNT composites prepared via electrostatic assembly and mortar mixing. In both composites, only peaks attributed to the base material were observed. This indicates that each material is stable in MeOH.

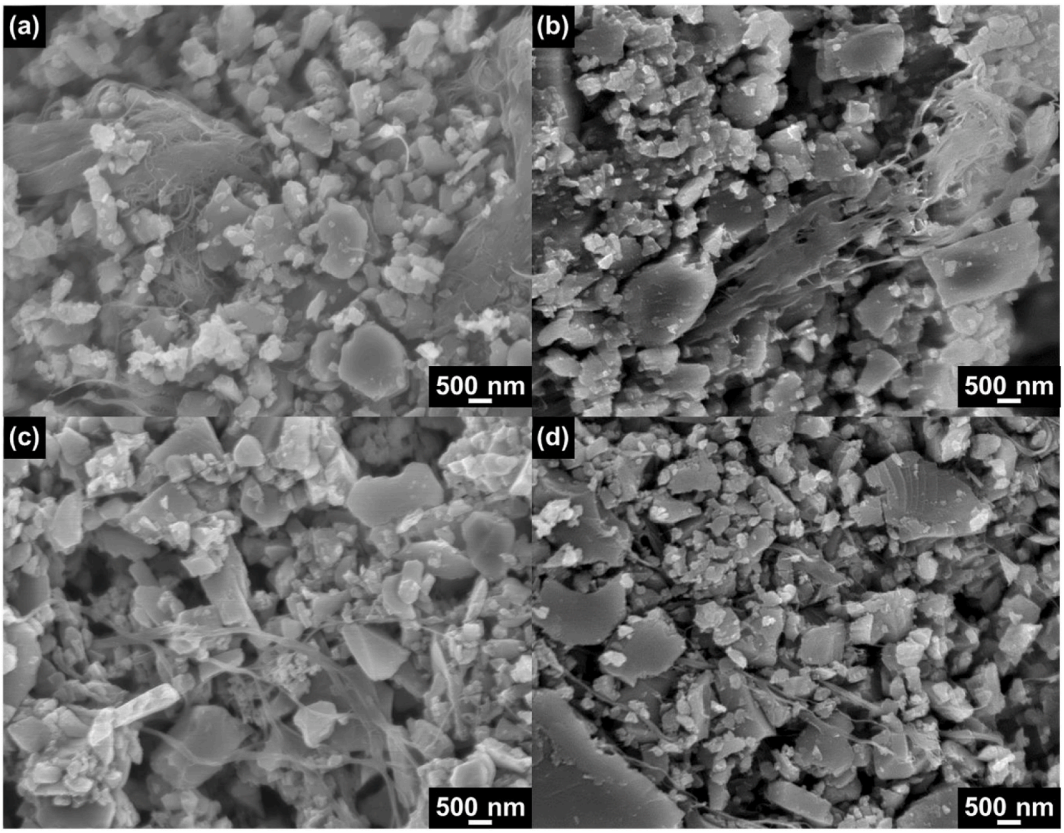

Fig. 1. (a) NMC–LATP–CNT and (b) LNMO–LATP–CNT composites obtained via mortar mixing; (c) NMC–LATP–CNT and (d) LNMO–LATP–CNT composites obtained via the electrostatic assembly method. The light gray color particles are LATP, the dark gray color particles are NMC or LNMO, and the fiber form is CNT.

3.2. Effect of sintering temperature

To estimate the optimal sintering temperature, cathode composites prepared via mortar mixing were sintered at various temperatures (650, 750, and 800 °C). Figs. 3 and S3 show the cross-sectional SEM images of NMC–LATP–CNT and LNMO–LATP–CNT composites at sintering temperatures of 650, 750, and 800 °C, respectively. Both composites appeared to be in a similar state after sintering at each temperature. At 650 °C (Figs. 3(a) and S3(a)), negligible particle necking was observed. At 750 °C (Figs. 3(b) and S3 (b)), the particles were observed to be rounded, and necks were formed at some locations. For 800 °C (Figs. 3(c) and S3(c)), grain growth and neck formation were distinctly visible.

Table 1 list the electronic and ionic conductivities of the NMC–LATP–CNT and LNMO–LATP–CNT composites at each sintering temperature, respectively. The electronic and ionic conductivities were calculated from the slopes of the approximate curve obtained from the I–V plots shown in Figs. S4 and S5 as obtained from the DC polarization tests, and the surface area and thickness of each sintered composite. Both composites presented the highest electronic conductivities at 650 °C, which decreased monotonically with increasing sintering temperature. In contrast, the ionic conductivities were the lowest at 650 °C and increased monotonically with increasing sintering temperature. In addition, no significant difference was observed at 750 and 800 °C. Considering these results, the side reaction between the cathode active material and LATP possibly occurred during sintering; therefore, the optimal sintering temperature was determined as 750 °C. The decrease in electronic conductivity and increase in ionic conductivity with increasing sintering temperature are attributed to the following reasons: Because CNTs decompose at approximately 600 °C at the atmosphere including oxygen [20], the partial reaction of CNTs with a small amount of oxygen included in the cathode composites during sintering at 750 °C or higher is considered to result in the partial burnout of CNTs inside the composites, thereby decreasing the electronic conductivity. However, for the ionic conductivity, at 650 °C, the grain boundary resistance between the solid electrolyte particle is high and the ionic conductivity becomes low. The simultaneous increase in the interfacial contact with the increasing sintering temperature consequently increases the ionic conductivity.

3.3. Properties comparison of the cathodes obtained using electrostatic integrated method and mortar mixing

Cathode composites prepared via mortar mixing and electrostatic integrated assembly were compared in terms of electronic and ionic conductivities. Table 2 present the electronic and ionic conductivities of the NMC–LATP–CNT and LNMO–LATP–CNT composites, respectively, for each mixing method. The cathodes fabricated using the electrostatic integrated powders exhibited higher electronic conductivity by two orders of magnitude for the NMC–LATP–CNT composite and by six orders of magnitude for the LNMO–LATP–CNT composite. The dispersion of CNTs in the cathode composite was enhanced, resulting in percolation of e^- path even at 1 wt% CNT (approximately 2.5 vol%). Furthermore, although the CNT addition ratio in the NMC–LATP–CNT and LNMO–LATP–CNT composites was equal, the electronic conductivities of the composites prepared via mortar mixing were relatively low, at 3.2×10^{-5} and 2.3×10^{-9} S cm^{-1} for the NMC–LATP–CNT and the LNMO–LATP–CNT composites, respectively. The insignificant improvement of electronic conductivity compared to NMC (10^{-6} S cm^{-1}) [21] and LNMO (10^{-9} S cm^{-1}) [22] without CNT addition was due to poor CNT dispersion and agglomeration, inhibiting the formation of electronic conductive pathway. In contrast, the NMC–LATP–CNT and LNMO–LATP–CNT composites prepared via the electrostatic integration method exhibited electronic conductivities of 6.5×10^{-3} and 6.4×10^{-3} S cm^{-1}, respectively. These results suggest that a uniform dispersion within the composites was obtained via electrostatic integrated assembly of the particles [23,24]. Moreover, the ionic conductivities of both composites were reduced by one order of magnitude for the composites prepared via electrostatic integration. The ratio of active material to solid electrolyte in the cathode composites is 1:2 (wt%), or approximately 1:3 (vol%). The solid electrolyte ratio inside the composite is 75%; therefore, the ionic conductivity is constant regardless of the mixing method.

To investigate the effect of the electrostatic integration technique in terms of the ionic conductivity, the electronic and ionic conductivities were evaluated by decreasing the solid electrolyte ratio. Fig. S6 shows the I–V plots from DC polarization tests of two samples with different mixing ratios (NMC:LATP:CNT = 44.5:44.5:1 and 69.3:29.7:1 (wt%)). Table 3 lists the measured electronic and ionic conductivities of the NMC–LATP–CNT composites for each mixing ratio. The electronic conductivity was constant for all mixing

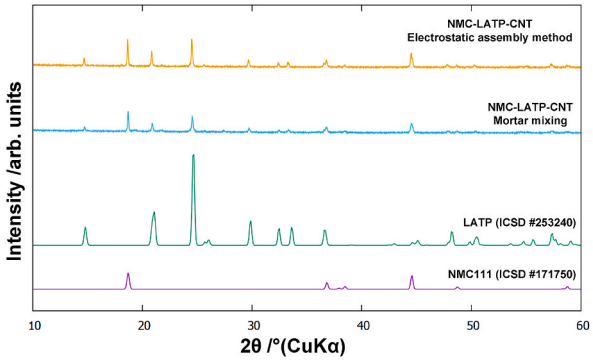

Fig. 2. X-ray diffraction patterns of NMC–LATP–CNT composites prepared through the electrostatic assembly method and mortar mixing.

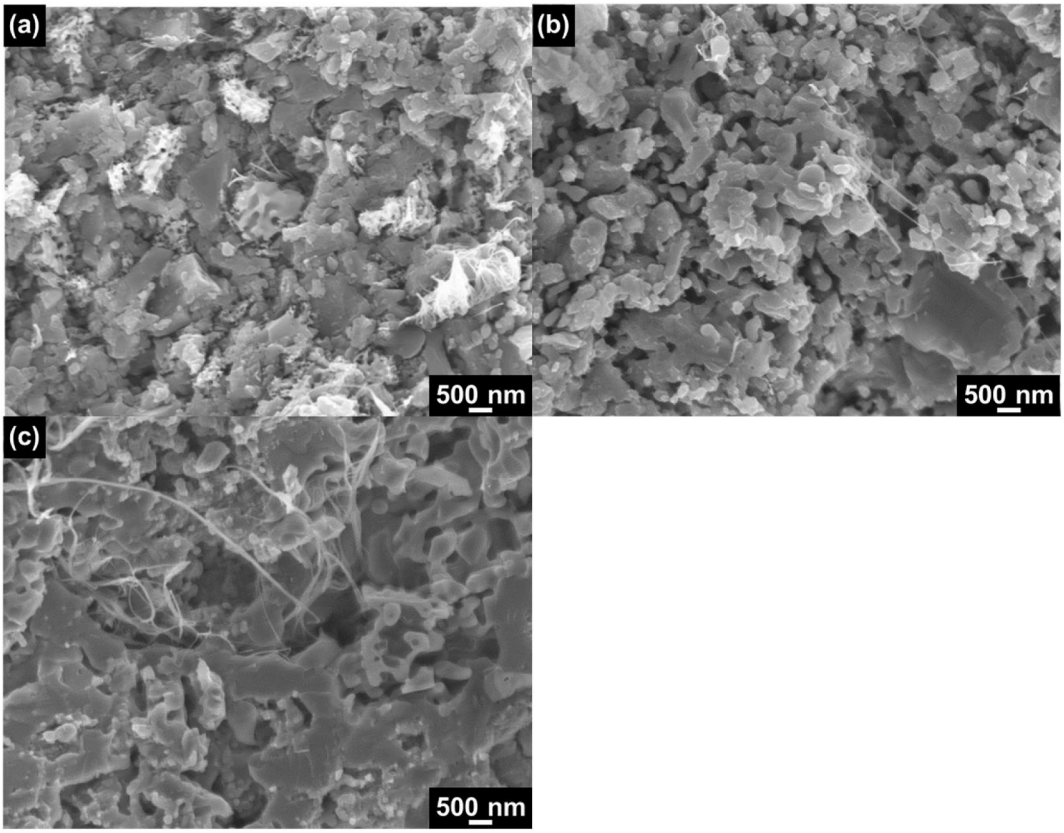

Fig. 3. Scanning electron microscopy images of NMC–LATP–CNT composites sintered at (a) 650, (b) 750, and (c) 800 °C.

Table 1
Electronic and ionic conductivities of NMC–LATP–CNT and LNMO–LATP–CNT composites sintered at 650, 750, and 800 °C.

Sintered temperature [°C]	Electronic conductivity [S cm^{-1}] of NMC/LNMO–LATP–CNT composites	Ionic conductivity [S cm^{-1}] of NMC/LNMO –LATP–CNT composites
650	$8.9 \times 10^{-4}/8.2 \times 10^{-5}$	$2.6 \times 10^{-7}/8.9 \times 10^{-7}$
750	$3.2 \times 10^{-5}/2.3 \times 10^{-9}$	$5.3 \times 10^{-5}/2.3 \times 10^{-5}$
800	$1.4 \times 10^{-5}/1.9 \times 10^{-9}$	$7.1 \times 10^{-5}/3.0 \times 10^{-5}$

Table 2
Electronic and ionic conductivities of NMC–LATP–CNT and LNMO–LATP–CNT composites fabricated through different methods and sintered at 750 °C.

Mixing method	Electronic conductivity [S cm^{-1}] of NMC/LNMO–LATP–CNT composites	Ionic conductivity [S cm^{-1}] of NMC/LNMO–LATP–CNT composites
Mortar mixing	$3.2 \times 10^{-5}/2.3 \times 10^{-9}$	$5.3 \times 10^{-5}/2.3 \times 10^{-5}$
Electrostatic integrated assembly	$6.5 \times 10^{-3}/6.4 \times 10^{-3}$	$6.5 \times 10^{-6}/1.4 \times 10^{-6}$

Table 3
Electronic and ionic conductivities of NMC–LATP–CNT composites prepared via the electrostatic assembly method at different mixing rates and sintered at 750 °C.

Mixing rate [wt%] NMC : LATP : CNT	Electronic conductivity [S cm^{-1}]	Ionic conductivity [S cm^{-1}]
33: 66: 1	6.5×10^{-3}	1.4×10^{-5}
44.5: 44.5: 1	1.9×10^{-2}	2.7×10^{-6}
69.3: 29.7: 1	9.5×10^{-2}	2.9×10^{-6}

ratios owing to the similar ratio of CNTs in all samples. However, the ionic conductivity decreased by one order of magnitude when the mixing ratio was changed from NMC:LATP:CNT = 33:66:1 (wt%) to 44.5:44.5:1 (wt%). The ionic conductivity decreased owing to the decrease in the content of LATP as an ionic conductor. However, comparing 44.5:44.5:1 (wt%) and 69.3:29.7:1 (wt%), the ionic conductivity was maintained in the order of 10^{-6} even at 69.3:29.7:1 (wt%), where the LATP content was decreased, because a more uniform mixture of LATP within the composite increases the efficient use of ionic conductor. This result suggests that electrostatic integration may decrease the amount of LATP to be added while maintaining ionic conductivity. NMC:LATP:CNT = 69.3:29.7:1 (wt%) is similar to the ratio of cathode composites in all-solid-state batteries. Therefore, this study indicates that cathode composites for oxide-type all-solid-state batteries can be fabricated with particles that are uniformly mixed via electrostatic interaction. Although this study focused on the electronic conductivity of cathode composites obtained through the electrostatic integrated assembly method, further investigation is necessary to increase the ionic conductivity through an improved sintering method such as sintering additive coating, applying spark plasma sintering for oxide-type all-solid-state battery applications [25,26]. In addition, it is also necessary to consider the combination of cathode active materials and solid electrolytes, because the low-temperature instability at $LiCoO_2$/LATP interface (≈400 °C), which is similar to NMC, has been reported in previous literatures [27,28].

4. Conclusions

Cathode composites were fabricated using two types of cathode active materials. Based on the SEM images of the obtained composites, we confirmed that CNTs could be uniformly dispersed in the composites via electrostatic integration. Subsequently, the composites were sintered at 650, 750, and 800 °C, and the optimal sintering temperature was determined by measuring the electronic and ionic conductivities of each sintered composite. The sintered composites exhibited the highest electronic conductivity sintered at 650 °C. Sintering at higher than 750 °C, the electronic conductivity decreased owing to the decomposition of CNTs. The ionic conductivity was the lowest sintered at 650 °C, and the value increased as sintering proceeded above 750 °C. To confirm that the improved dispersion of materials via electrostatic integration improves the electrochemical properties, the electronic and ionic conductivities of cathode composites prepared via electrostatic integration and mortar mixing were measured. Electrostatic integration increased the electronic conductivity due to improved CNT distribution. In the composites with different mixing ratios, we confirmed that the ionic conductivity was maintained in the composites with a reduced solid electrolyte addition ratio. Thus, integrated cathode composites for oxide-type all-solid-state batteries exhibiting uniform dispersibility and efficient materials usage can be fabricated via electrostatic interaction. Although these cathode active materials cannot be effectively used in organic electrolyte-based batteries, the study findings can contribute to expand the application from thin-film-type to practical powder-type all-solid-state batteries using high-performance cathode active materials.

Author contribution statement

Kazuhiro Hikima: Conceived and designed the experiments; Analyzed and interpreted the data; Contributed reagents, materials, analysis tools or data; Wrote the paper.

Yusaku Sato: Conceived and designed the experiments; Performed the experiments; Analyzed and interpreted the data; Contributed reagents, materials, analysis tools or data.

Atsushi Yokoi: Conceived and designed the experiments; Performed the experiments; Contributed reagents, materials, analysis tools or data.

Wai Kian Tan, Hiroyuki Muto, Atsunori Matsuda: Contributed reagents, materials, analysis tools or data.

Data availability statement

Data will be made available on request.

Declaration of competing interest

The authors declare that they have no known competing financial interests or personal relationships that could have appeared to influence the work reported in this paper.

Acknowledgements

This study was supported by the Japanese Society for the Promotion of Science KAKENHI (Grant No. JP 21K14716), Kazuchika Okura memorial foundation, Naito Science & Engineering Foundation, and Toyota Riken Scholar Program.

Appendix A. Supplementary data

Supplementary data to this article can be found online at https://doi.org/10.1016/j.heliyon.2023.e17889.

References

[1] K. Hikima, M. Totani, S. Obokata, H. Muto, A. Matsuda, ACS Appl. Energy Mater. 5 (2022) 2349–2355.
[2] N. Kamaya, K. Homma, Y. Yamakawa, M. Hirayama, R. Kanno, M. Yonemura, T. Kamiyama, Y. Kato, S. Hama, K. Kawamoto, A. Mitsui, Nat. Mater. 10 (2011) 682.
[3] F. Mizuno, A. Hayashi, K. Tadanaga, M. Tatsumisago, Electrochem. Solid State Lett. 8 (2005) A603.
[4] K. Hikima, K. Suzuki, S. Taminato, M. Hirayama, S. Yasuno, R. Kanno, Chem. Lett. 48 (2019) 192–195.
[5] K. Hikima, K. Shimizu, H. Kiuchi, Y. Hinuma, K. Suzuki, M. Hirayama, E. Matsubara, R. Kanno, Commun. Chem. 5 (2022).
[6] K. Hikima, K. Shimizu, H. Kiuchi, Y. Hinuma, K. Suzuki, M. Hirayama, E. Matsubara, R. Kanno, J. Am. Chem. Soc. 144 (2022) 236–247.
[7] K. Waetzig, A. Rost, C. Heubner, M. Coeler, K. Nikolowski, M. Wolter, J. Schilm, J. Alloys Compd. (2020) 818.
[8] L. Hallopeau, D. Bregiroux, G. Rousse, D. Portehault, P. Stevens, G. Toussaint, C. Laberty-Robert, J. Power Sources 378 (2018) 48–52.
[9] J.P. Beaupain, K. Waetzig, S.-K. Otto, A. Henss, J. Janek, M. Malaki, A. Pokle, J. Müller, B. Butz, K. Volz, M. Kusnezoff, A. Michaelis, ACS Appl. Mater. Interfaces 13 (2021) 47488–47498.
[10] W.K. Tan, N. Hakiri, A. Yokoi, G. Kawamura, A. Matsuda, H. Muto, Nanoscale Res. Lett. 14 (2019).
[11] H. Muto, A. Yokoi, W.K. Tan, J. Comp. Sci. 4 (2020).
[12] H. Muto, Y. Sato, W.K. Tan, A. Yokoi, G. Kawamura, A. Matsuda, Nanoscale 14 (2022) 9669–9674.
[13] S. Hasegawa, N. Imanishi, T. Zhang, J. Xie, A. Hirano, Y. Takeda, O. Yamamoto, J. Power Sources 189 (2009) 371–377.
[14] H. Aono, J. Electrochem. Soc. 136 (1989) 590.
[15] H. Aono, E. Sugimoto, Y. Sadaoka, N. Imanaka, G.y. Adachi, J. Electrochem. Soc. 137 (1990) 1023–1027.
[16] J.S. Thokchom, B. Kumar, J. Electrochem. Soc. 154 (2007) A331.
[17] L. Li, R. Zhao, T. Xu, D. Wang, D. Pan, K. Zhang, C. Yu, X. Lu, G. He, Y. Bai, Nanoscale 11 (2019) 8967–8977.
[18] M.A. Pogosova, I.V. Krasnikova, A.O. Sanin, S.A. Lipovskikh, A.A. Eliseev, A.V. Sergeev, K.J. Stevenson, Chem. Mater. 32 (2020) 3723–3732.
[19] N.H.H. Phuc, M. Takaki, M. Hiroyuki, M. Atsunori, Front. Energy Res. 8 (2021).
[20] K. Mukul, A. Yoshinori, Defence Sci. J. 58 (2008) 496–503.
[21] J. Zahnow, T. Bernges, A. Wagner, N. Bohn, J.R. Binder, W.G. Zeier, M.T. Elm, J. Janek, ACS Appl. Energy Mater. 4 (2021) 1335–1345.
[22] R. Amin, I. Belharouk, J. Power Sources 348 (2017) 311–317.
[23] W.K. Tan, Y. Matsubara, A. Yokoi, G. Kawamura, A. Matsuda, I. Sugiyama, N. Shibata, Y. Ikuhara, H. Muto, Adv. Powder Technol. (2022) 33.
[24] T. Akatsu, Y. Takiguchi, Y. Shinoda, F. Wakai, H. Muto, Ceram. Int. 48 (2022) 36515–36520.
[25] K. Ishii, M. Ode, K. Mitsuishi, S. Miyoshi, T. Ohno, K. Takada, T. Uchikoshi, J. Power Sources 546 (2022).
[26] T. Okumura, T. Takeuchi, H. Kobayashi, Electrochemistry 82 (2014) 906–908.
[27] S. Muto, Y. Yamamoto, M. Sakakura, H.-K. Tian, Y. Tateyama, Y. Iriyama, ACS Appl. Energy Mater. 5 (2021) 98–107.
[28] H.-K. Tian, R. Jalem, B. Gao, Y. Yamamoto, S. Muto, M. Sakakura, Y. Iriyama, Y. Tateyama, ACS Appl. Mater. Interfaces 12 (2020) 54752–54762.

Glossary

CNT: Carbon nanotube
LATP: $Li_{1.3}Al_{0.3}Ti_{1.7}(PO_4)_3$
LNMO: $LiNi_{0.5}Mn_{1.5}O_4$
NMC: $LiNi_{1/3}Mn_{1/3}Co_{1/3}O_2$
PDDA: Poly(diallydimethyl ammonium chloride
SEM: Scanning electron microscopy